# The Peroxisomal Enzyme L-PBE Is Required to Prevent the Dietary Toxicity of Medium-Chain Fatty Acids

Jun Ding,[1,6] Ursula Loizides-Mangold,[2,6] Gianpaolo Rando,[1] Vincent Zoete,[3] Olivier Michielin,[3] Janardan K. Reddy,[4] Walter Wahli,[1,5] Howard Riezman,[2,7,*] and Bernard Thorens[1,7,*]

[1]Center for Integrative Genomics, University of Lausanne, Lausanne 1015, Switzerland
[2]Department of Biochemistry, NCCR Chemical Biology, University of Geneva, 1211 Geneva, Switzerland
[3]Swiss Institute for Bioinformatics, University of Lausanne, 1015 Lausanne, Switzerland
[4]Department of Pathology, Northwestern University, Chicago, IL 60611, USA
[5]Lee Kong Chian School of Medicine, Nanyang Technological University, Singapore 639798, Singapore
[6]These authors contributed equally to this work
[7]These authors contributed equally to this work
*Correspondence: howard.riezman@unige.ch (H.R.), bernard.thorens@unil.ch (B.T.)
http://dx.doi.org/10.1016/j.celrep.2013.08.032

## SUMMARY

Specific metabolic pathways are activated by different nutrients to adapt the organism to available resources. Although essential, these mechanisms are incompletely defined. Here, we report that medium-chain fatty acids contained in coconut oil, a major source of dietary fat, induce the liver ω-oxidation genes *Cyp4a10* and *Cyp4a14* to increase the production of dicarboxylic fatty acids. Furthermore, these activate all ω- and β-oxidation pathways through peroxisome proliferator activated receptor (PPAR) α and PPARγ, an activation loop normally kept under control by dicarboxylic fatty acid degradation by the peroxisomal enzyme L-PBE. Indeed, *L-pbe*$^{-/-}$ mice fed coconut oil overaccumulate dicarboxylic fatty acids, which activate all fatty acid oxidation pathways and lead to liver inflammation, fibrosis, and death. Thus, the correct homeostasis of dicarboxylic fatty acids is a means to regulate the efficient utilization of ingested medium-chain fatty acids, and its deregulation exemplifies the intricate relationship between impaired metabolism and inflammation.

## INTRODUCTION

The liver plays a critical role in lipid metabolism with multiple enzymatic pathways controlling lipid uptake, modifications, catabolism, as well as lipid biosynthesis and export. The routes followed by fatty acids to reach the liver and the adaptation of liver lipid metabolism differ according to fatty acid chain length. Following their uptake by enterocytes, long- and very-long-chain fatty acids ($\geq$C14) are re-esterified into triglycerides and incorporated into chylomicrons. These are transported via lymph vessels into the blood to distribute fatty acids to peripheral tissues.

Chylomicron remnants are eventually taken up by the liver (Williams, 2008). In contrast to this indirect pathway, medium-chain fatty acids (C8–C12) are taken up by enterocytes and directly transported through the hepatoportal circulation to the liver for uptake and degradation (Papamandjaris et al., 1998). Thus, hepatocytes must be able to cope with rapid and potentially massive influxes of medium-chain fatty acids. Coconut oil, a major source of fat for millions of people living mainly in tropical areas, but also an important component of several processed foods, consists mainly of medium-chain fatty acids with a particularly high abundance of lauric acid (Kumar, 2011). The impact of coconut oil feeding on health is still debated. Because it contains high amounts of saturated fat, it is considered potentially harmful for health. On the other hand, many studies indicate that it has beneficial effects (DebMandal and Mandal, 2011; Houssay and Martínez, 1947). The lack of knowledge concerning the molecular mechanisms and physiology associated with coconut oil consumption still prevents a clear understanding of its potential impact on health.

In a previous study aimed at identifying lipid metabolic pathways associated with resistance to coconut oil high-fat (HFD-CO)-induced hepatic steatosis and liver inflammation, we identified the peroxisomal enzyme enoyl-CoA hydratase/L-3-hydroxyacyl-CoA dehydrogenase (*Ehhadh*) (also called L-peroxisomal bifunctional enzyme, *L-pbe*, the term used in this study) as a potential protection gene (Hall et al., 2010). L-PBE catalyzes the second and third steps of peroxisomal β-oxidation, reactions also catalyzed by the enzyme D-PBE (D-peroxisomal bifunctional enzyme, *Hsd17b4*) (Reddy and Hashimoto, 2001). Whereas D-PBE is constitutively expressed, L-PBE is inducible (Wanders and Waterham, 2006), and the enzymes have different substrate specificities. Genetic inactivation of *Hsd17b4* induces growth retardation and prevents very-long-chain fatty acid oxidation and bile acid maturation (Baes et al., 2000). In contrast, mice with genetic inactivation of *L-pbe* have no obvious phenotype (Qi et al., 1999), and the range of substrates for this enzyme is not fully established. Here, we investigated the specific role of
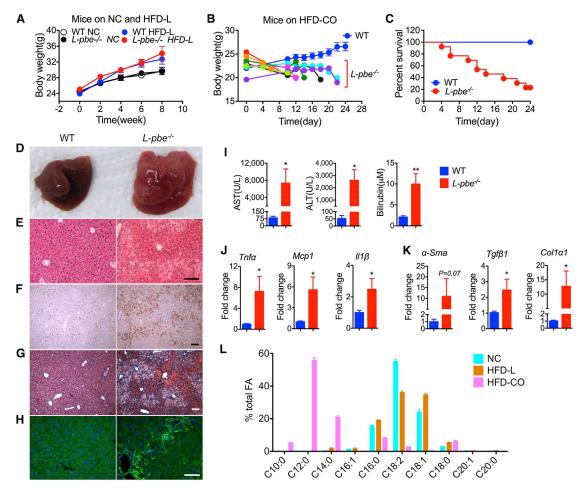
**Figure 1. *L-pbe*<sup>−/−</sup> Mice Develop Fulminant Liver Failure When Fed a HFD-CO but Not HFD-L**

(A) Growth curves of WT and *L-pbe*<sup>−/−</sup> mice on normal chow (NC) and HFD-L. NC group: WT, n = 10; *L-pbe*<sup>−/−</sup> n = 12. HFD-L: WT, n = 10; *L-pbe*<sup>−/−</sup> n = 8.

(B) Change in body weight of WT (n = 5) and *L-pbe*<sup>−/−</sup> (n = 8) mice fed a HFD-CO.

(C) Survival curve of WT (n = 9) and *L-pbe*<sup>−/−</sup> (n = 13) mice fed a HFD-CO.

(D) Livers from WT and *L-pbe*<sup>−/−</sup> mice fed a HFD-CO.

(E) Hematoxylin and eosin staining.

(F) F4/80 immunostaining.

(G) Masson's trichrome staining.

(H) α-Smooth muscle actin immunostaining of liver sections. Scale bars, 100 μm.

(I) Blood levels of aspartate (AST), alanine (ALT) aminotransferases, and bilirubin.

(J and K) Hepatic expression levels of (J) mRNAs for proinflammatory cytokines and (K) fibrosis markers. Values are means ± SEM, n = 6.

(L) Analysis of the fatty acid content of the three different diets; HFD-CO is highly enriched in medium-chain fatty acids with lauric acid representing about 50% total fatty acids.

See also Figures S1, S2, and S3.

L-PBE in the adaptation to HFD-CO feeding and demonstrated its role in regulating the amount of medium-chain dicarboxylic fatty acids, which are essential activators of all fatty acid oxidation pathways and whose accumulation correlates with liver failure.

## RESULTS

### Coconut Oil, but Not Lard, Induces Weight Loss and Death in *L-pbe*<sup>−/−</sup> Mice

*L-pbe*<sup>−/−</sup> mice fed a normal chow (NC) are phenotypically indistinguishable from their wild-type littermates (Qi et al., 1999)

(Figure 1A, for body weight). However, when fed a HFD-CO diet, the *L-pbe*<sup>−/−</sup> mice rapidly lost weight and most of them died within 3 weeks, whereas wild-type mice gained weight and remained healthy (Figures 1B and 1C). In initial studies, we also compared wild-type with *L-pbe*<sup>+/−</sup> and *L-pbe*<sup>−/−</sup> littermates. No phenotype could be observed in HFD-CO-fed heterozygous mice, and in the rest of the study we only compared wild-type and *L-pbe*<sup>−/−</sup> mice.

Because mouse milk is rich in C16 and C18 triglycerides (Smith et al., 1968) and *L-pbe*<sup>−/−</sup> mice grew normally during the suckling period, the lipid species rather than the amount of

fat absorbed may have caused death of the *L-pbe*$^{-/-}$ mice. To test this hypothesis, we fed *L-pbe*$^{-/-}$ mice a lard-based HFD (HFD-L) and saw that these mice gained weight normally and remained healthy (Figure 1A). These results indicate that *L-pbe* is required selectively for the adaptation to HFD-CO.

### Fulminant Liver Failure in HFD-CO-Fed *L-pbe*$^{-/-}$ Mice

To assess the cause of death in HFD-CO-fed *L-pbe*$^{-/-}$ mice, we analyzed them shortly before death, when they were severely sick or when their original body weight was reduced by ∼25%. Histological examination of different organs revealed no abnormalities in heart, lung, kidneys, or stomach (Figure S1). However, the livers of the HFD-CO-fed mice were larger (Figure 1D) and characterized by hepatocyte ballooning, macrophage infiltration, and increased fibrosis as revealed by collagen and smooth muscle actin staining (Figures 1E–1H). Increased hepatocyte proliferation and apoptosis were also visible (Figures S2A and S2B). The presence of liver failure was confirmed by the strongly increased plasma levels of aspartate (AST) and alanine (ALT) aminotransferases and of bilirubin (Figure 1I). Liver inflammation was associated with increased expression of the mRNAs for the inflammatory cytokines tumor necrosis factor α (*Tnfα*), monocyte chemoattractant protein 1 (*Mcp-1*), and interleukin-1β (*Il-1β*) (Figure 1J). Increased expression of the mRNAs for alpha smooth muscle actin (*α-Sma*), transforming growth factor beta 1 (*Tgfβ1*), and collagen type I alpha 1 (*Col1α1*) confirmed development of fibrosis (Figure 1K). Total liver triglycerides, free cholesterol, and cholesteryl esters were not different between HFD-CO-fed control and *L-pbe*$^{-/-}$ mice (Figures S2C and S2D). Biochemical analysis of the plasma of HFD-CO-fed *L-pbe*$^{-/-}$ mice showed higher concentrations of TNFα and MCP-1 as well as slightly increased cholesterol and free fatty acid (FA) levels, elevated LDL and diminished HDL, and hypoglycemia, with normal insulin levels (Table S1).

Presence of oxidative stress was demonstrated by increased hepatic levels of the lipid peroxidation products 4-hydroxynonenal (4-HNE) and malondialdehyde (MDA) (Figures S2E and S2F) and by increased expression of antioxidant, phase II genes, including the glutathione-related enzymes (glutathione reductase [*Gsr*], glutathione S-transferase μ1 and μ3 [*Gstμ1* and *Gstμ3*], glutamate-cysteine ligase catalytic subunit [*Gclc*], heme oxygenase-1 [*Hmox1*], and the NAD[P]H:quinone oxidoreductase 1 [*Nqo1*]) (Figure S2G). Ceramides, which are also associated with oxidative stress, as well as glycosylceramides, showed markedly elevated levels in the livers of HFD-CO-fed *L-pbe*$^{-/-}$ mice, whereas sphingomyelin levels were normal (Figures S2H and S2I). The sphingolipid synthesis genes, including subunits of serine palmitoyltransferases (*Spt1* and *Spt2*), ceramide synthases 4 and 6 (*CerS4* and *CerS6*), ceramide δ(4)-desaturase (*Des1*), and the glucosylceramide synthase (*Gcs*) were also markedly elevated (Figure S2J).

No alteration in liver histology, evidence of liver damage, increased inflammation, or fibrosis could be observed in *L-pbe*$^{-/-}$ mice fed for 2 weeks with a lard-based HFD (Table S1; Figures S3A–S3G).

Collectively, these data indicated that death of HFD-CO-fed *L-pbe*$^{-/-}$ mice was a consequence of liver inflammation, fibrosis, and failure but was not associated with liver steatosis.

Furthermore, none of these effects were seen when mice were fed a lard-based HFD.

### *L-pbe* Deficiency Leads to Dicarboxylic Fatty Acid Accumulation

Lipidomic analysis of NC, HFD-CO, and HFD-L (Figure 1L) showed absence of very-long-chain FAs (>C20) in either diet; long-chain FAs (C16 and C18) were the major species in HFD-L and NC, whereas HFD-CO predominantly consisted of the medium-chain fatty acids (MCFAs) decanoic (C10), lauric (C12), and myristic (C14) acids with lauric acid representing ∼50% of total FAs.

As a first step to identify why the HFD-CO caused the observed liver phenotype, we assessed the expression of key enzymes involved in fatty acid oxidation, i.e., in mitochondrial and peroxisomal β-oxidation and in microsomal ω-oxidation. In NC-fed mice, mitochondrial β-oxidation (medium-chain acyl-CoA dehydrogenase [*Mcad*], long-chain acyl-CoA dehydrogenase [*Lcad*], and trifunctional protein alpha subunit [*Hadhα*]), peroxisomal β-oxidation (acyl-coenzyme A oxidase 1 [*Acox1*], *Hsd17b4*, thiolase B [*Acaa1b*]), and microsomal ω-oxidation (cytochrome P450 family 4 subfamily a polypeptide 10 and 14, *Cyp4a10* and *Cyp4a14*) genes were expressed at similar levels in wild-type and *L-pbe*$^{-/-}$ mice (Figure 2A). After 2 days of HFD-CO feeding, there was a small increase in the expression of the peroxisomal β oxidation gene *Acaa1b* and a strong induction of ω-oxidation genes in the *L-pbe*$^{-/-}$ mouse livers (Figure 2B). After long-term HFD-CO feeding, all the mitochondrial, peroxisomal, and microsomal fatty acid oxidation (FAO) genes were significantly induced (Figure 2C).

The above data show that among the genes tested *Cyp4a*s were the first and most induced genes. These encode microsomal cytochromes (CYP4A10 and CYP4A14) that are responsible for the first step in the production of dicarboxylic fatty acids (DCAs) by ω-oxidation (Hardwick, 2008). Lipidomic analysis revealed a striking accumulation of DCAs in the livers of HFD-CO-fed *L-pbe*$^{-/-}$ mice with dodecanedioic acid (C12DCA) being the most induced species, both after 2 days or long-term HFD-CO feeding (Figures 2D–2F). Figure S4A shows the relative amounts of the different DCA species extracted from livers of wild-type mice fed a HFD-CO. No accumulation of lauric acid was seen in the livers of *L-pbe*$^{-/-}$ mice fed a NC or a HFD-CO (Figures S4B and S4C), and no difference in hepatic acyl-CoA or phospholipid contents could be observed in control or *L-pbe*$^{-/-}$ mice (Figures S4D and S4E).

Thus, the immediate increase in *Cyp4a* expression and the accumulation of dicarboxylic fatty acids were early events in the liver pathology. As DCAs are normally degraded in the peroxisomes (Suzuki et al., 1989), these data suggested that L-PBE was required for their degradation. Previous studies have indeed proposed that DCAs are preferential substrates for L-PBE (Dirkx et al., 2007; Ferdinandusse et al., 2004; Houten et al., 2012; Nguyen et al., 2008). These studies have been performed using C10, C14, C16, and C20DCAs as substrates. Here, we measured the rate of degradation of C12DCA in liver homogenates from wild-type and *L-pbe*$^{-/-}$ mice. This analysis showed a significantly higher rate of degradation of C12DCA in control as compared to *L-pbe*$^{-/-}$ liver homogenates (Figure 2G), with faster
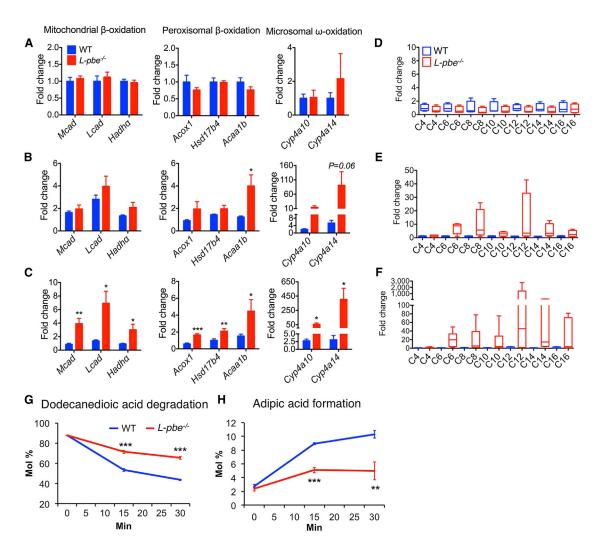
**Figure 2. HFD-CO Induces Fatty Acid β- and ω-Oxidation Pathways and the Accumulation of DCAs in the Livers of *L-pbe*⁻/⁻ Mice**

(A–C) mRNA levels of fatty acid oxidation genes were measured in the livers of (A) NC-fed mice, (B) after 2 days of HFD-CO feeding, and (C) after long-term HFD-CO feeding.

(D–F) DCA accumulation in the livers of NC or HFD-CO-fed mice corresponding to (A)–(C), respectively. Values are means ± SEM (n = 6), *p < 0.05, **p < 0.01, and ***p < 0.001.

(G and H) (G) Degradation rate of dodecanedioic acid (C12DCA) and (H) appearance of its degradation product adipic acid (C6DCA) in liver homogenates from WT and *L-pbe*⁻/⁻ mice. One representative out of three independent experiments is shown.

Values are means ± SEM (n = 3), **p < 0.01 and ***p < 0.001. See also Figure S4 and Table S1.

rates of appearance of the C12DCA degradation products C10, C8, C6, C4, and C3DCAs as shown for adipic acid (C6DCA) (Figure 2H; data not shown) (Jin and Tserng, 1991).

To provide an independent indication of the role of medium-chain fatty acids in inducing liver failure, we fed wild-type and *L-pbe*⁻/⁻ mice for 5 days with a NC complemented with 25% glyceryl trilaurate. In *L-pbe*⁻/⁻ mice. This induced body weight loss, alteration of liver histology, increased plasma AST and ALT, increased hepatic expression of phase II and sphingolipid synthesis genes, of the inflammatory and fibrosis markers *Tnfα*, *Mcp1*, *Il-1β*, *Tgfβ1*, *α-Sma*, and *Col1α1*, as well as of *Cyp4a10* and *Cyp4a14* (Figures 3A–3H). These defects were also associated with increased hepatic accumulation of DCAs (Figure 3I). Importantly, DCAs larger than C12 were induced by

glyceryl trilaurate feeding, showing that the induction of ω-oxidation mobilizes fat from sources other than the C12 triglyceride.

Together, the above observations indicate that the toxic effect of coconut oil on *L-pbe*⁻/⁻ mouse livers is replicated by lauric acid feeding and is associated with the rapid accumulation of DCAs, which are normally degraded by L-PBE.

**Lauric Acid and DCAs Activate Peroxisome Proliferator Activated Receptors and Fatty Acid Oxidation Pathways**

The fatty acid oxidation genes measured in Figures 2A–2C are typical peroxisome proliferator activated receptor (PPAR) targets (Pyper et al., 2010). To determine whether HFD-CO indeed induced a greater activation of PPARs in *L-pbe*⁻/⁻ than wild-type mice, we transfected the liver of mice using a hydrodynamic
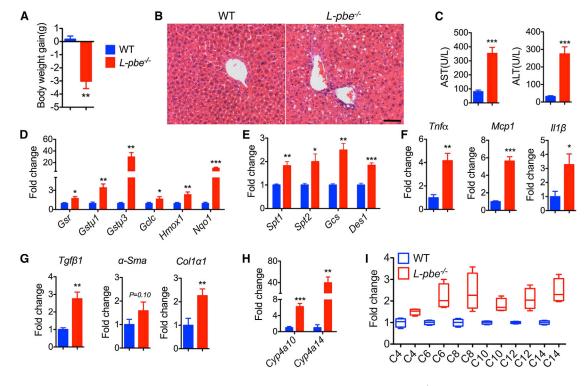
**Figure 3. Glyceryl-Trilaurate-Supplemented Normal Chow Diet Induces Liver Damage in *L-pbe*$^{-/-}$ Mice**

(A–G) WT and *L-pbe*$^{-/-}$ mice were fed a NC complemented with glyceryl trilaurate for 5 days and the following analysis were performed. (A) Change in body weight. (B) Hematoxylin and eosin staining of liver sections. (C) Plasma AST and ALT levels. (D) Hepatic expression of phase II genes. (E) Sphingolipid biosynthesis genes. (F) mRNAs for proinflammatory cytokines. (G) Fibrosis markers of WT and *L-pbe*$^{-/-}$ mice.

(H) *Cyp4a10* and *Cyp4a14* expression levels.

(I) Hepatic accumulation of DCAs.

Values are means ± SEM (n = 6), *p < 0.05, **p < 0.01, and ***p < 0.001.

delivery system with a plasmid containing a peroxisome proliferator response elements (PPREs) driving the expression of a luciferase reporter gene. Mice were then fed a NC or HFD-CO, and luciferase activity was monitored on 3 consecutive days. Luciferase activity was much higher in HFD-CO-fed *L-pbe*$^{-/-}$ mice than wild-type mice, whereas there was no difference in luciferase activity between the two types of mice on NC (Figures 4A and 4B).

Because the PPRE reporter plasmid used in these experiments can be activated by PPARα and PPARγ, we assessed the hepatic expression of PPARs under the different feeding conditions. Figures 4C–4E show that upon HFD-CO feeding expression of PPARα in the livers of *L-pbe*$^{-/-}$ mice was unchanged; PPARβ/δ was induced only after long-term HFD-CO feeding, and PPARγ expression was rapidly induced in 2 days and much more after long-term feeding. This suggests that the in vivo transcriptional response (Figure 4A) may be controlled by different PPARs at different times after initiation of HFD-CO feeding.

To determine whether lauric acid and DCAs were activators of PPARs, we performed a transactivation assay using Gal4-ligand binding domain-luciferase reporter constructs. We found that lauric acid could induce PPARα and PPARγ transcriptional activity, and also mildly activate PPARβ/δ (Figure 4F). Furthermore, we showed that C12DCA and C16DCA could activate both

PPARα and PPARγ (Figure 4G). Molecular modeling of the binding mode of C12DCA and C16DCA to the ligand binding sites of human PPARs showed a more optimal binding of C16DCA than C12DCA or lauric acid to PPARα and PPARγ. This involves one carboxylate group binding the polar head of the ligand binding domain (S317, H351, H477, and Y501 in PPARγ) with the other carboxylate possibly interacting with R308; this double interaction of carboxylates is more difficult to establish with the shorter C12DCA (Figures S5A and S5B). Due to the strong sequence identity among important residues of the human and the mouse isoforms of the proteins (see Table S2), we can expect that the differences in the calculated binding modes found between isoforms of human PPARs will be conserved between isoforms of mouse PPARs.

Collectively, these data show that lauric acid and DCAs can activate PPARα and PPARγ and that PPARγ expression is rapidly induced in the liver of HFD-CO-fed *L-pbe*$^{-/-}$ mice. Thus, in the absence of L-PBE-dependent degradation of DCAs, these induce a feedforward mechanism to increase the PPAR-dependent expression of all fatty oxidation pathways.

## DCAs Mediate the Toxic Effect of Coconut Oil

To determine if DCAs mediate the toxic effect of coconut oil, we fed *L-pbe*$^{-/-}$ mice with C12DCA-supplemented NC. After a 4 day feeding period, *L-pbe*$^{-/-}$ mice lost more than 6 g of
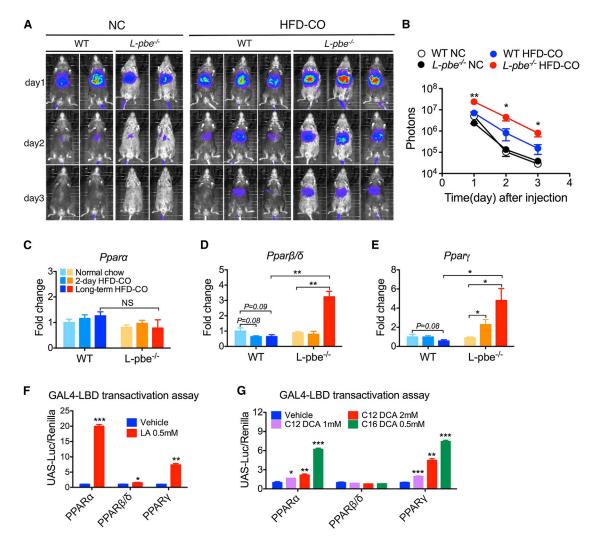
**Figure 4. HFD-CO, Lauric Acid, and DCAs Activate PPARα and PPARγ**

(A) Luciferase activity measured in WT or $L$-$pbe^{-/-}$ mice expressing a PPRE-luciferase reporter construct in their liver and fed a NC or HFD-CO. Luciferase activity was recorded at the indicated times after transfection of the reporter construct.

(B) Quantification of the luciferase activity. Data are means ± SEM, n = 5 for the NC groups and n = 7 for the HFD-CO groups. *p < 0.05, **p < 0.01, and ***p < 0.001.

(C–E) Expression of PPARα, PPARβ/δ, and PPARγ in the liver of WT or $L$-$pbe^{-/-}$ mice fed a NC or HFD-CO, as indicated. Values are means ± SEM (n = 6), *p < 0.05, **p < 0.01, and ***p < 0.001.

(F and G) Transactivation of the mentioned PPAR (ligand binding domain of mouse PPARα, mouse PPARβ/δ, or human PPARγ) reporter constructs by (F) lauric acid and (G) C12 and C16 DCAs.

Values are means ± SEM (n = 4), *p < 0.05, **p < 0.01, and ***p < 0.001. See also Figure S5 and Table S2.

body weight, whereas wild-type mice lost ∼1 g (Figure 5A). Histological analysis demonstrated severe liver damage in the $L$-$pbe^{-/-}$ mice as well as massively increased plasma AST and ALT levels (Figures 5B–5D). This was also associated with marked induction of the liver mRNAs for phase II proteins, sphingolipid synthesis enzymes, and cytokines (Figures 5E–5G). In agreement with the transcriptional regulatory activity of DCAs, 1 day of C12DCA-supplemented diet feeding induced mitochondrial, peroxisomal, and microsomal FAO pathways (Figures 5H–5J), with a striking >30-fold induction of $L$-$pbe$ in wild-type mouse livers supporting that L-PBE is a major enzyme required for adaptation to this DCA feeding. Also remarkable was the

60- to >100-fold induction of $Cyp4a$s in $L$-$pbe^{-/-}$ mice, further supporting our proposal that DCAs induce a positive feedback loop between CYP4A enzymatic products and expression of these enzymes.

To test whether inhibiting DCA production would prevent liver failure, we fed $L$-$pbe^{-/-}$ mice for 3 weeks a HFD-CO with simultaneous treatment with 1-aminobenzotriazole (ABT), an inhibitor of CYP4As (Isayama et al., 2003; Kaikaus et al., 1993; Kroetz and Xu, 2005). This treatment suppressed the production of DCAs (Figure 6A), allowed survival of the mice (Figure 6B), and protected them against liver failure, as shown by their normal plasma AST and ALT levels (Figure 6C) and normal liver histology
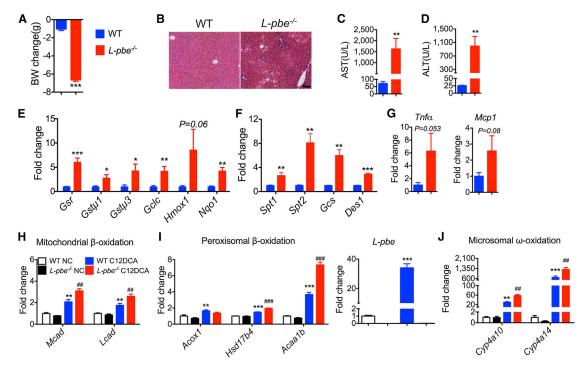
**Figure 5. C12DCA-Supplemented Normal Chow Induces Liver Failure in *L-pbe*$^{-/-}$ Mice**

(A–G) Four days after initiation of C12DCA feeding, liver failure was evident as shown by the following. (A) Loss of body weight. (B) Liver histology. (C and D) Plasma AST and ALT levels. (E) Antioxidant genes expression. (F) Sphingolipid synthesis gene expression. (G) Cytokine gene expression. Scale bars, 100 μm. Values are means ± SEM (WT, n = 5; *L-pbe*$^{-/-}$, n = 7–12), *p < 0.05, **p < 0.01, and ***p < 0.001.

(H–J) Fatty acid oxidation gene expression in the liver of WT and *L-pbe*$^{-/-}$ mice fed a NC or a C12DCA-supplemented NC diet for 1 day. Values are means ± SEM (n = 6). WT NC versus WT C12DCA, *p < 0.05, **p < 0.01, and ***p < 0.001; *L-pbe*$^{-/-}$ C12DCA versus WT C12DCA, #p < 0.05, ##p < 0.01, and ###p < 0.001.

(Figure S6A). The treatment also prevented the induction of phase II, sphingolipid synthesis, and inflammatory cytokines genes (Figures S6B–S6D).

As ABT may also inhibit other enzymes than CYP4As, we specifically silenced their activity by tail vein injection of small interfering RNA (siRNAs) directed toward *Cyp4a10* and *Cyp4a14* mRNAs. This treatment suppressed both *Cyp4a10* and *Cyp4a14* expression (Figure 6D) and the production of DCAs (Figure 6E) and markedly improved the survival of HFD-CO-fed *L-pbe*$^{-/-}$ mice (Figure 6F). This treatment also prevented liver damage as revealed by normal liver histology, plasma AST, and ALT levels and absence of induction of phase II, sphingolipid synthesis, and inflammatory cytokines genes (Figures S6E–S6I).

Finally, as a further control that DCAs are the downstream product of CYP4As that are relevant to the phenotype, we fed *L-pbe*$^{-/-}$ mice a C12DCA-supplemented diet and simultaneously treated them with ABT. *L-pbe*$^{-/-}$ mice with or without ABT treatment showed similar phenotypes after 3 day C12DCA-supplemented diet feeding as shown by their similar loss in body weight (Figure S6J), showing that ABT prevents the liver phenotype through inhibition of CYP4A-dependent DCA synthesis.

The above data confirm our model that DCA production by CYP4A activity in HFD-CO-fed *L-pbe*$^{-/-}$ mice leads to hepatic failure and death.

## DISCUSSION

Here, we describe a liver regulatory mechanism that is required to prevent the dietary toxicity of MCFAs. This mechanism (Figure 6G) involves the induction by MCFAs of CYP4As leading to an increased production of DCAs. These activate, in a PPARα/PPARγ-dependent manner, the expression of CYP4As as well as the expression of mitochondrial and peroxisomal fatty acid β-oxidation genes. We show that genetic inactivation of the peroxisomal enzyme L-PBE leads to intracellular DCA accumulation, inflammation, fibrosis, and liver failure. Thus, our data suggest that the balance between DCA production by CYP4As and their degradation by L-PBE is a mechanism that normally fine-tunes hepatic β- and ω-oxidation activities in response to MCFA absorption. An imbalance between these mechanisms may cause massive nutrient-induced inflammation.

Several beneficial effects of MCFAs as compared to long-chain fatty acids have been described when added as food complement, notably a reduction of different aspects of the metabolic syndrome (Papamandjaris et al., 1998; St-Onge et al., 2003, 2008), in part by increasing energy expenditure and reducing fat mass and by preventing development of insulin resistance (Rubin et al., 2000; Turner et al., 2009). The way by which MCFAs increase energy expenditure and FAO appears to be related to their ability to activate PPARs. Two recent reports demonstrated that MCFAs can activate PPARγ, PPARα,
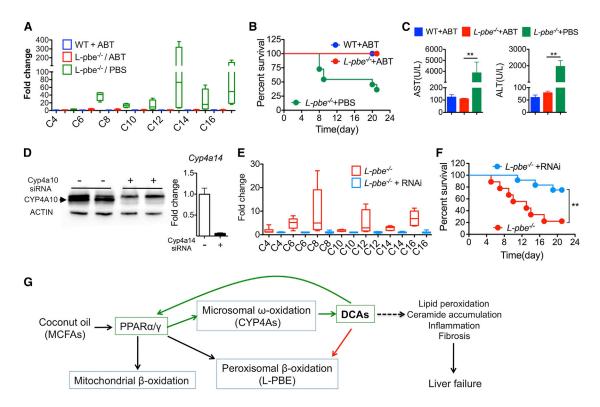
**Figure 6. Preventing DCA Production by Suppressing CYP4A Activity Protects against Liver Failure**

(A–C) WT or *L-pbe*$^{-/-}$ mice were fed a HFD-CO and treated with the CYP4 inhibitor ABT or with PBS. (A) ABT treatment suppressed DCA formation, (B) protected the mice from death, and (C) normalized plasma AST and ALT levels. PBS group: WT, n = 5; *L-pbe*$^{-/-}$, n = 11. ABT group: WT, n = 5; *L-pbe*$^{-/-}$, n = 13.

(D) Western blot analysis of CYP4A10 and mRNA level of *Cyp4a14* in the livers of fasted mice treated with *Cyp4a* specific or control siRNAs.

(E and F) DCA levels (E) and survival curves (F) of HFD-CO-fed *L-pbe*$^{-/-}$ mice treated with *Cyp4a* specific or control siRNAs. *L-pbe*$^{-/-}$, n = 9; *L-pbe*$^{-/-}$ +RNAi, n = 12. Values are means ± SEM. **p < 0.01.

(G) Schematic description of the mechanism by which coconut oil (MCFAs) induces CYP4A-dependent production of DCAs. DCAs then activate a feedforward mechanism to further activate the three fatty oxidation pathways. This feedforward loop is normally regulated by L-PBE-dependent DCA degradation. In the absence of L-PBE, accumulation of DCAs leads to liver failure through the induction of inflammation and fibrosis.

See also Figure S6.

and PPARβ/δ and can reduce adipogenesis in a cellular model of adipocyte differentiation (Liberato et al., 2012; Malapaka et al., 2012). In agreement with these publications, we show that lauric acid can transactivate PPARα and PPARγ and, consequently, liver FAO pathways in the liver (Patsouris et al., 2006; Peters et al., 2003). We show that feeding of mice with glyceryl trilaurate induces ω-oxidation of other fat sources than the C12 triglyceride. This suggests that the pathway of ω-oxidation of MCFAs is used to stimulate reduction of fat mass in general and is not only a specific mechanism to deal with MCFAs.

The transcriptional response to lauric acid includes increased expression of *Cyp4a*s, which preferentially use this fatty acid as a substrate to initiate its conversion to dodecanedioic acid (C12DCA) (Adas et al., 1999; Hardwick, 2008). In the absence of the L-PBE, a DCA degrading enzyme, there is accumulation of DCAs in the liver. These are good transcriptional activators of both PPARα and PPARγ, providing an explanation for the observation that DCAs can induce FAO (Fan et al., 1998; Lundgren et al., 1992). Also, as compared to lauric acid, DCAs are relatively better activators of PPARγ than PPARα, and C16DCA is more potent than C12DCA. This can be understood

in the context of our results showing that MCFAs induce ω-oxidation from a variety of fat sources increasing DCAs of all chain lengths. It is remarkable that the induction of *L-pbe* and *Cyp4a*s in vivo by C12DCA feeding of wild-type mice was about 40- and >100-fold, respectively. This was a more robust induction than seen in the in vitro PPRE-luciferase reporter assay, suggesting that some of the DCAs or other oxidation intermediates produced in vivo by the C12DCA-induced ω-oxidation pathway are better activators of PPARs. Less likely, it could be that the sensitivity of the luciferase reporter assay is less than the sensitivity of the endogenous transcription regulatory system. Also, because HFD-CO feeding increases expression of *Pparβ/δ* and *Pparγ*, the full activation by DCAs of FAO pathways involves the combined control of PPAR expression and transcriptional activity.

Thus, our data indicate that rapidly after coconut oil, or glyceryl trilaurate ingestion, MCFAs absorbed by the liver first activate PPARα. This is rapidly followed by induction of microsomal ω-oxidation and formation of DCAs. These then more strongly activate PPARα and PPARγ, whose expression becomes markedly induced. This feedforward loop accelerates induction of

FAO pathways (Figure 6G). These observations suggest that formation of DCAs by ω-oxidation upon MCFA feeding is an adaptive mechanism to rapidly induce all FA disposal mechanisms. Under normal conditions, only ~10%–20% of the MCFAs absorbed by the liver are channeled through microsomal ω-oxidation (Björkhem, 1978; Handler and Thurman, 1988), supporting that this may be a regulatory rather than a major degradation pathway. It is interesting to note that DCAs have been proposed as potential drugs for diabetes treatment (Mingrone et al., 2012). Our data suggest that this may be mediated by their capacity to induce PPAR transcriptional activity and activate all FAO pathways.

An important aspect of our study is the demonstration that accumulation of DCAs caused by the genetic inactivation of *L-pbe* leads to massive inflammation, fibrosis, and liver failure. The mechanisms by which DCAs, or some of their metabolites, induce this reaction, is still unknown. However, earlier studies showed that medium-chain DCAs can inhibit mitochondrial respiration and reduce ATP production by affecting electron transfer reactions (Passi et al., 1984; Tonsgard and Getz, 1985), thus favoring reactive oxygen species (ROS) production. Increased peroxisomal β-oxidation also contributes to the production of ROS. This oxidative stress may explain the accumulation of lipid peroxidation products, which are chemoattractants for inflammatory cells (Curzio et al., 1985). Increased ceramide production is also a sign of cellular stress and inflammation (Bikman and Summers, 2011), and ceramides can uncouple oxidative phosphorylation leading to increased leakage of electrons to generate ROS and induce apoptosis (Corda et al., 2001; Li et al., 2010). Thus, the inflammatory and fibrotic response to HFD-CO feeding may combine several, cross-amplifying mechanisms.

Whether the deregulation of this adaptive mechanism may cause liver diseases in humans is still to be discovered. However, a recent study reported association of SNPs in the *L-PBE* gene with elevated fasting serum insulin and plasma glucose levels (Banasik et al., 2011), parameters that are highly influenced by inflammation (Glass and Olefsky, 2012), and a genome-wide association study identified CYP4A as a risk locus for hepatic steatosis (Suhre et al., 2011). Further studies in humans may uncover a clearer link between MCFA-rich diets and liver inflammation in the context of individual genetic susceptibilities. It is, however, interesting to note that MCAD deficiency, a disease caused by homozygous inactivation of the mitochondrial medium-chain acyl-CoA dehydrogenase gene (*MCAD* or *ACADM*), can cause acute hypoketotic hypoglycemia, lethargy, seizures, and coma leading to sudden death, a condition that is associated with hepatomegaly, acute liver disease, and urine secretion of C6, C8, and C10DCAs (Feillet et al., 2003; Schatz and Ensenauer, 2010). This condition is favored by fasting suggesting that, in absence of *MCAD*, MCFAs are channeled to *CYP4A*s to generate excessive DCAs causing conditions similar to that observed in HFD-CO-fed mice.

Thus, collectively, our data show that the physiological function of the peroxisomal enzyme L-PBE is to degrade medium-chain dicarboxylic acids whose role is to induce all FAO pathways in response to MCFA feeding. This represents an unsuspected mechanism required to adapt liver metabolism to the ingestion of a specific type of lipid. This also demonstrates that impaired medium-chain fatty acid metabolism may rapidly induce an inflammatory reaction that can have fatal consequences.

## EXPERIMENTAL PROCEDURES

### Mice and Diets

*L-pbe*$^{-/-}$ mice from a mixed 129/Ola-C57Bl/6 background have been previously described (Qi et al., 1999). For our initial studies, *L-pbe*$^{-/-}$ mice were crossed with C57Bl/6 mice to generate *L-pbe*$^{+/-}$ mice, which were then intercrossed to obtain *L-pbe*$^{+/+}$(WT), *L-pbe*$^{+/-}$, and *L-pbe*$^{-/-}$ littermates. Mice were maintained at 24°C on a 12-hr/12-hr-light/dark cycle (7:00–19:00), with free access to water and NC (3436 from Provimi Kliba AG) and were used when 6–8 weeks old. Only male mice were used for the experiments presented here. For HFD feeding, mice were fed with coconut-oil-based HFD (HFD-CO) or lard-based HFD (HFD-L) (D12331 and D12492 from Research Diets). The customized diets were prepared by grinding the normal chow (3436 from Provimi Kliba) and mixing with glyceryl trilaurate (Yacoo) to 25% (w/w) and dodecanedioic acid (C12DCA) (Sigma-Aldrich) to 10% (w/w).

*L-pbe*$^{-/-}$ mice fed a HFD-CO were killed when they were severely sick (markedly reduced mobility and feeding behavior) or had lost 25% of their original body weight (long-term feeding). Wild-type mice were killed after 21–24 day feeding. In feeding experiments, all mice were killed in the fed state. Blood samples were collected by heart puncture in EDTA and aprotinin (Sigma-Aldrich). Liver samples were rapidly dissected, weighed, frozen in liquid nitrogen, and stored at −80°C. All animal studies were approved by the Veterinary Office of Canton de Vaud, Switzerland.

1-Aminobenzotriazole (ABT) (Sigma-Aldrich) was dissolved in PBS and gavaged at 100 mg/kg/day, which has been shown to be effective to inhibit lauric acid hydroxylase activity in mice (Isayama et al., 2003; Kaikaus et al., 1993). All treatments started simultaneously with the food shift.

### Histology and Immunohistochemistry

Livers were fixed with 4% paraformaldehyde and embedded in paraffin, and 5 μm sections were prepared for hematoxylin and eosin or Masson's trichrome staining. Immunofluorescence microscopy was performed using antibodies against F4/80 (Abcam), α-smooth muscle actin (Sigma-Aldrich), Ki67 (Abcam), cleaved caspase 3 (Cell Signaling Technology), and 4-HNE (Jaica) according to the manufacturer's instructions. Malondialdehyde (MDA) was measured with the TBARS Assay Kit by following manufacturer's protocol (Cayman Chemical). Other tissues were examined with similar procedures.

### Analysis of Dicarboxylic Acids

Extraction and analysis of dicarboxylic fatty acids was adapted from Kushnir et al. (2001). Briefly, 15 mg of ground liver tissue was resuspended in 1 ml $H_2O$. One hundred microliters of an internal standard (1 μmol/l methyl malonic acid [MMA]) and 3 ml of MTBE containing 30 ml/l phosphoric acid were added. Samples were vortexed for 5 min and centrifuged. The supernatant was transferred to a new glass tube and dried under a flow of nitrogen. One hundred sixty microliters of HCl (3 M) in 1-butanol was added. The mixture was incubated at 50°C for 5 min. Samples were dried under nitrogen and then resuspended with 300 μl methanol containing 50 ml/l ammonium formate. Analysis of dicarboxylic fatty acids was achieved by a liquid chromatography system equipped with an Uptisphere Strategy C18-2 high-performance liquid chromatography (HPLC) column (Interchim) coupled to a Varian 320-MS triple quadrupole mass spectrometer (Agilent Technologies) or a TSQ Vantage triple quadrupole mass spectrometer (Thermo). Mass spectrometer settings of selected dicarboxylic fatty acids are shown in Table S3.

### RNA Extraction and Real-Time PCR

Total RNA was prepared from livers using RNA Stat-60 according to the manufacturer's instructions (Amsbio). First-strand cDNA was synthesized from 2.5 μg of total RNA using random primers (Promega) and Superscript II reverse transcriptase (Invitrogen). Real-time PCR was performed using Power SYBR Green Master Mix (Applied Biosystems). All reactions were normalized to

β2-microglobulin (B2M) levels. Specific mouse primers for each gene are listed in Table S4.

## Analysis of Fatty acyl-CoAs

Fatty acyl-CoAs were extracted from 15 mg ground liver tissue. Each sample was resuspended in 200 μl water and spiked with 10 μl of an internal standard mix (100 pmol of C15:0-, C17:0-, C23:0-, C25:0-CoA, Avanti Polar Lipids). Fatty acyl-CoA extraction and analysis were performed as described (Haynes et al., 2008). HPLC separation was achieved on a Gemini C18 column (150 × 2 mm column size, 5 μm particle size, Phenomenex). Mass spectrometry analysis was done on a Varian 320-MS Triple Quadrupole Mass Spectrometer (Agilent Technologies) equipped with an ESI source. Mass spectrometer settings of selected fatty acyl-CoAs are listed in Table S5.

## Luciferase Assay in Cell Culture

Gal4-ligand binding domain of mouse PPARα, mouse PPARβ/δ, or human PPARγ plasmids were gifts from B. Staels (Université Lille Nord de France, Lille, France) and Johan Auwerx (École polytechnique fédérale de Lausanne). The 5x-UAS-TK-Luc was purchased from Promega. The NIH 3T3 mouse fibroblasts in 12-well plates were transiently transfected with 0.8 μg of DNA: Gal4-LBD, 5x-UAS-TK-Luc, and CMV Renilla. Lauric acid and C12DCA were dissolved in sodium hydroxide for the stock solution (100 and 200 mM, respectively), bound to fatty-acid-free BSA (1 mM fatty acid to 1% BSA), and then added to the medium for 24 hr. Luciferase assay was performed with Dual-luciferase reporter assay system (Promega). Firefly luciferase activity was normalized to CMV Renilla luciferase.

## Hydrodynamic Injection

The hydrodynamic injection was performed as previously described with small modifications (Bell et al., 2007). Briefly, 10 mg/ml PPRE (L-pbe promoter, position −2952 to −2918)-luciferase plasmid (Bardot et al., 1993) (generously provided by C. Carlberg) solution was prepared and intravenously injected in ~5 s to the mice based on body weight (10% v/w). After injection and full recovery, mice were divided into NC- and HFD-CO-fed groups. Mice were then injected with luciferin and anesthetized with isoflurane, and luciferase activity was measured using an in vivo bioluminescence imaging system (Xenogen IVIS 3D, Caliper).

## β-Oxidation Measurements

β-Oxidation measurements were described elsewhere (Hall et al., 2010) with small modifications. Mice were fasted for 24 hr before liver collection. C12DCA (0.5 mM) was added to the reactions, which were incubated at 37°C and then snap frozen in liquid nitrogen at different time points. Fatty acid oxidation or formation rates were analyzed after lipid profiling.

## In Vivo siRNA Treatment

RNAi siRNA duplexes (Ambion and Invitrogen) complementary to the Cyp4a10 and Cyp4a14 genes were complexed with Invivofectamine 2.0 (Invitrogen) according to manufacturer recommendation before the injection. For each gene, two to four siRNAs with different sequences were tested, and that yielding maximal suppression was selected for the experiments. An equimolar mix of the two Cyp4a siRNAs or control siRNA was injected intravenously through the tail vein of 6-week-old mice at a dose of 7 mg/kg. After 7–10 days HFD-CO feeding, the same injection was performed again.

## Statistics

Statistical analysis was performed with Student's t test. Quantitative data are expressed as mean ± SEM. p values less than 0.05 were considered significant. Other statistical methods were mentioned and indicated where they were used.

For additional details, see the Extended Experimental Procedures.

## SUPPLEMENTAL INFORMATION

Supplemental Information includes Extended Experimental Procedures, six figures, and five tables and can be found with this article online at http://dx.doi.org/10.1016/j.celrep.2013.08.032.

## REFERENCES

Adas, F., Berthou, F., Salaün, J.P., Dréano, Y., and Amet, Y. (1999). Interspecies variations in fatty acid hydroxylations involving cytochromes P450 2E1 and 4A. Toxicol. Lett. 110, 43–55.

Baes, M., Huyghe, S., Carmeliet, P., Declercq, P.E., Collen, D., Mannaerts, G.P., and Van Veldhoven, P.P. (2000). Inactivation of the peroxisomal multifunctional protein-2 in mice impedes the degradation of not only 2-methyl-branched fatty acids and bile acid intermediates but also of very long chain fatty acids. J. Biol. Chem. 275, 16329–16336.

Banasik, K., Justesen, J.M., Hornbak, M., Krarup, N.T., Gjesing, A.P., Sandholt, C.H., Jensen, T.S., Grarup, N., Andersson, A., Jørgensen, T., et al. (2011). Bioinformatics-driven identification and examination of candidate genes for non-alcoholic fatty liver disease. PLoS ONE 6, e16542.

Bardot, O., Aldridge, T.C., Latruffe, N., and Green, S. (1993). PPAR-RXR heterodimer activates a peroxisome proliferator response element upstream of the bifunctional enzyme gene. Biochem. Biophys. Res. Commun. 192, 37–45.

Bell, J.B., Podetz-Pedersen, K.M., Aronovich, E.L., Belur, L.R., McIvor, R.S., and Hackett, P.B. (2007). Preferential delivery of the Sleeping Beauty transposon system to livers of mice by hydrodynamic injection. Nat. Protoc. 2, 3153–3165.

Bikman, B.T., and Summers, S.A. (2011). Ceramides as modulators of cellular and whole-body metabolism. J. Clin. Invest. 121, 4222–4230.

Björkhem, I. (1978). On the quantitative importance of omega-oxidation of fatty acids. J. Lipid Res. 19, 585–590.

Corda, S., Laplace, C., Vicaut, E., and Duranteau, J. (2001). Rapid reactive oxygen species production by mitochondria in endothelial cells exposed to tumor necrosis factor-alpha is mediated by ceramide. Am. J. Respir. Cell Mol. Biol. 24, 762–768.

Curzio, M., Esterbauer, H., and Dianzani, M.U. (1985). Chemotactic activity of hydroxyalkenals on rat neutrophils. Int. J. Tissue React. 7, 137–142.

DebMandal, M., and Mandal, S. (2011). Coconut (Cocos nucifera L.: Arecaceae): in health promotion and disease prevention. Asian Pac J Trop Med 4, 241–247.

Dirkx, R., Meyhi, E., Asselberghs, S., Reddy, J., Baes, M., and Van Veldhoven, P.P. (2007). Beta-oxidation in hepatocyte cultures from mice with peroxisomal gene knockouts. Biochem. Biophys. Res. Commun. 357, 718–723.

Fan, C.Y., Pan, J., Usuda, N., Yeldandi, A.V., Rao, M.S., and Reddy, J.K. (1998). Steatohepatitis, spontaneous peroxisome proliferation and liver tumors in mice lacking peroxisomal fatty acyl-CoA oxidase. Implications for peroxisome proliferator-activated receptor alpha natural ligand metabolism. J. Biol. Chem. 273, 15639–15645.

Feillet, F., Steinmann, G., Vianey-Saban, C., de Chillou, C., Sadoul, N., Lefebvre, E., Vidailhet, M., and Bollaert, P.E. (2003). Adult presentation of MCAD deficiency revealed by coma and severe arrythmias. Intensive Care Med. 29, 1594–1597.

Ferdinandusse, S., Denis, S., Van Roermund, C.W., Wanders, R.J., and Dacremont, G. (2004). Identification of the peroxisomal beta-oxidation enzymes

involved in the degradation of long-chain dicarboxylic acids. J. Lipid Res. *45*, 1104–1111.

Glass, C.K., and Olefsky, J.M. (2012). Inflammation and lipid signaling in the etiology of insulin resistance. Cell Metab. *15*, 635–645.

Hall, D., Poussin, C., Velagapudi, V.R., Empsen, C., Joffraud, M., Beckmann, J.S., Geerts, A.E., Ravussin, Y., Ibberson, M., Oresic, M., and Thorens, B. (2010). Peroxisomal and microsomal lipid pathways associated with resistance to hepatic steatosis and reduced pro-inflammatory state. J. Biol. Chem. *285*, 31011–31023.

Handler, J.A., and Thurman, R.G. (1988). Catalase-dependent ethanol oxidation in perfused rat liver. Requirement for fatty-acid-stimulated H2O2 production by peroxisomes. Eur. J. Biochem. *176*, 477–484.

Hardwick, J.P. (2008). Cytochrome P450 omega hydroxylase (CYP4) function in fatty acid metabolism and metabolic diseases. Biochem. Pharmacol. *75*, 2263–2275.

Haynes, C.A., Allegood, J.C., Sims, K., Wang, E.W., Sullards, M.C., and Merrill, A.H., Jr. (2008). Quantitation of fatty acyl-coenzyme As in mammalian cells by liquid chromatography-electrospray ionization tandem mass spectrometry. J. Lipid Res. *49*, 1113–1125.

Houssay, B.A., and Martínez, C. (1947). Experimental Diabetes and Diet. Science *105*, 548–549.

Houten, S.M., Denis, S., Argmann, C.A., Jia, Y., Ferdinandusse, S., Reddy, J.K., and Wanders, R.J. (2012). Peroxisomal L-bifunctional enzyme (Ehhadh) is essential for the production of medium-chain dicarboxylic acids. J. Lipid Res. *53*, 1296–1303.

Isayama, F., Froh, M., Bradford, B.U., McKim, S.E., Kadiiska, M.B., Connor, H.D., Mason, R.P., Koop, D.R., Wheeler, M.D., and Arteel, G.E. (2003). The CYP inhibitor 1-aminobenzotriazole does not prevent oxidative stress associated with alcohol-induced liver injury in rats and mice. Free Radic. Biol. Med. *35*, 1568–1581.

Jin, S.J., and Tserng, K.Y. (1991). Biogenesis of dicarboxylic acids in rat liver homogenate studied by 13C labeling. Am. J. Physiol. *261*, E719–E724.

Kaikaus, R.M., Chan, W.K., Lysenko, N., Ray, R., Ortiz de Montellano, P.R., and Bass, N.M. (1993). Induction of peroxisomal fatty acid beta-oxidation and liver fatty acid-binding protein by peroxisome proliferators. Mediation via the cytochrome P-450IVA1 omega-hydroxylase pathway. J. Biol. Chem. *268*, 9593–9603.

Kroetz, D.L., and Xu, F. (2005). Regulation and inhibition of arachidonic acid omega-hydroxylases and 20-HETE formation. Annu. Rev. Pharmacol. Toxicol. *45*, 413–438.

Kumar, S.N. (2011). Variability in coconut (Cocos nucifera L.) germplasm and hybrids for fatty acid profile of oil. J. Agric. Food Chem. *59*, 13050–13058.

Kushnir, M.M., Komaromy-Hiller, G., Shushan, B., Urry, F.M., and Roberts, W.L. (2001). Analysis of dicarboxylic acids by tandem mass spectrometry. High-throughput quantitative measurement of methylmalonic acid in serum, plasma, and urine. Clin. Chem. *47*, 1993–2002.

Li, X., Becker, K.A., and Zhang, Y. (2010). Ceramide in redox signaling and cardiovascular diseases. Cell. Physiol. Biochem. *26*, 41–48.

Liberato, M.V., Nascimento, A.S., Ayers, S.D., Lin, J.Z., Cvoro, A., Silveira, R.L., Martínez, L., Souza, P.C., Saidemberg, D., Deng, T., et al. (2012). Medium chain fatty acids are selective peroxisome proliferator activated receptor (PPAR) γ activators and pan-PPAR partial agonists. PLoS ONE *7*, e36297.

Lundgren, B., Andersson, K., and DePierre, J.W. (1992). Effects of dietary treatment with 11 dicarboxylic acids, diethylcarboxylic esters and fatty acids on peroxisomal fatty acid beta-oxidation, epoxide hydrolases and lauric acid omega-hydroxylation in mouse liver. Biochem. Pharmacol. *43*, 785–792.

Malapaka, R.R., Khoo, S., Zhang, J., Choi, J.H., Zhou, X.E., Xu, Y., Gong, Y., Li, J., Yong, E.L., Chalmers, M.J., et al. (2012). Identification and mechanism of 10-carbon fatty acid as modulating ligand of peroxisome proliferator-activated receptors. J. Biol. Chem. *287*, 183–195.

Mingrone, G., Castagneto-Gissey, L., and Mace, K. (2012). Use of dicarboxylic acids in type 2 diabetes. Br. J. Clin. Pharmacol. *75*, 671–676.

Nguyen, S.D., Baes, M., and Van Veldhoven, P.P. (2008). Degradation of very long chain dicarboxylic polyunsaturated fatty acids in mouse hepatocytes, a peroxisomal process. Biochim. Biophys. Acta *1781*, 400–405.

Papamandjaris, A.A., MacDougall, D.E., and Jones, P.J. (1998). Medium chain fatty acid metabolism and energy expenditure: obesity treatment implications. Life Sci. *62*, 1203–1215.

Passi, S., Picardo, M., Nazzaro-Porro, M., Breathnach, A., Confaloni, A.M., and Serlupi-Crescenzi, G. (1984). Antimitochondrial effect of saturated medium chain length (C8-C13) dicarboxylic acids. Biochem. Pharmacol. *33*, 103–108.

Patsouris, D., Reddy, J.K., Müller, M., and Kersten, S. (2006). Peroxisome proliferator-activated receptor alpha mediates the effects of high-fat diet on hepatic gene expression. Endocrinology *147*, 1508–1516.

Peters, J.M., Aoyama, T., Burns, A.M., and Gonzalez, F.J. (2003). Bezafibrate is a dual ligand for PPARalpha and PPARbeta: studies using null mice. Biochim. Biophys. Acta *1632*, 80–89.

Pyper, S.R., Viswakarma, N., Yu, S., and Reddy, J.K. (2010). PPARalpha: energy combustion, hypolipidemia, inflammation and cancer. Nucl. Recept. Signal *8*, e002.

Qi, C., Zhu, Y., Pan, J., Usuda, N., Maeda, N., Yeldandi, A.V., Rao, M.S., Hashimoto, T., and Reddy, J.K. (1999). Absence of spontaneous peroxisome proliferation in enoyl-CoA Hydratase/L-3-hydroxyacyl-CoA dehydrogenase-deficient mouse liver. Further support for the role of fatty acyl CoA oxidase in PPARalpha ligand metabolism. J. Biol. Chem. *274*, 15775–15780.

Reddy, J.K., and Hashimoto, T. (2001). Peroxisomal beta-oxidation and peroxisome proliferator-activated receptor alpha: an adaptive metabolic system. Annu. Rev. Nutr. *21*, 193–230.

Rubin, M., Moser, A., Vaserberg, N., Greig, F., Levy, Y., Spivak, H., Ziv, Y., and Lelcuk, S. (2000). Structured triacylglycerol emulsion, containing both medium- and long-chain fatty acids, in long-term home parenteral nutrition: a double-blind randomized cross-over study. Nutrition *16*, 95–100.

Schatz, U.A., and Ensenauer, R. (2010). The clinical manifestation of MCAD deficiency: challenges towards adulthood in the screened population. J. Inherit. Metab. Dis. *33*, 513–520.

Smith, S., Watts, R., and Dils, R. (1968). Quantitative gas-liquid chromatographic analysis of rodent milk triglycerides. J. Lipid Res. *9*, 52–57.

St-Onge, M.P., Ross, R., Parsons, W.D., and Jones, P.J. (2003). Medium-chain triglycerides increase energy expenditure and decrease adiposity in overweight men. Obes. Res. *11*, 395–402.

St-Onge, M.P., Bosarge, A., Goree, L.L., and Darnell, B. (2008). Medium chain triglyceride oil consumption as part of a weight loss diet does not lead to an adverse metabolic profile when compared to olive oil. J. Am. Coll. Nutr. *27*, 547–552.

Suhre, K., Shin, S.Y., Petersen, A.K., Mohney, R.P., Meredith, D., Wägele, B., Altmaier, E., Deloukas, P., Erdmann, J., Grundberg, E., et al.; CARDIoGRAM. (2011). Human metabolic individuality in biomedical and pharmaceutical research. Nature *477*, 54–60.

Suzuki, H., Yamada, J., Watanabe, T., and Suga, T. (1989). Compartmentation of dicarboxylic acid beta-oxidation in rat liver: importance of peroxisomes in the metabolism of dicarboxylic acids. Biochim. Biophys. Acta *990*, 25–30.

Tonsgard, J.H., and Getz, G.S. (1985). Effect of Reye's syndrome serum on isolated chinchilla liver mitochondria. J. Clin. Invest. *76*, 816–825.

Turner, N., Hariharan, K., TidAng, J., Frangioudakis, G., Beale, S.M., Wright, L.E., Zeng, X.Y., Leslie, S.J., Li, J.Y., Kraegen, E.W., et al. (2009). Enhancement of muscle mitochondrial oxidative capacity and alterations in insulin action are lipid species dependent: potent tissue-specific effects of medium-chain fatty acids. Diabetes *58*, 2547–2554.

Wanders, R.J., and Waterham, H.R. (2006). Biochemistry of mammalian peroxisomes revisited. Annu. Rev. Biochem. *75*, 295–332.

Williams, K.J. (2008). Molecular processes that handle — and mishandle — dietary lipids. J. Clin. Invest. *118*, 3247–3259.

# Supplemental Information

## EXTENDED EXPERIMENTAL PROCEDURES

### Biochemical Analysis

Plasma TNFα, IL-1β, and MCP-1 were determined using Mouse Cytokine/Chemokine Panel (Millipore, Zug, Switzerland). AST and ALT were measured by enzymatic tests (Roche Applied Science, Basel, Switzerland) using a Hitachi robot 902.

### Triglyceride Levels in Liver

Mouse liver (~50 mg) was homogenized in chloroform:methanol (2:1) solution. Distilled water was added and mixed vigorously with the homogenate. After centrifugation, solvent phase was kept for the next column separation steps. SPE columns were purchased from Laubscher labs (Miecourt, Switzerland). Lipid extracts were eluted by chloroform, followed by drying and reconstitution with chloroform. For the determination of concentration, we used the Triglyceride enzymatic PAP 150 kit (Biomerieux, Geneva, Switzerland) by following the instructions.

### Chemicals and Lipid Standards

DLPC 12:0/12:0 (850335), PE 17:0/14:1 (PE31:1, LM-1104), PI 17:0/14:1 (PI31:1, LM-1504), PS 17:0/14:1 (PS31:1, LM-1304), C17:0 Ceramide (860517), C12:0 SM (860583), Glucosyl C8:0 Cer (860540) were used as internal lipid standards and were purchased from Avanti Polar Lipids Inc (Alabaster, Alabama, USA). Ergosterol was used as sterol standard and was purchased from Fluka (Buchs, Switzerland). Methylmalonic acid (MMA), hydrogen chloride (3 M in 1-butanol) and LC MS grade ammonium formate were purchased from Sigma-Aldrich. Phosphoric acid (85 wt % solution in water) was from Acros Organics (Thermo Scientific).

MTBE was from Fluka (Buchs, Switzerland). Methylamine (33% in absolute ethanol) was from Sigma-Aldrich. HPLC grade chloroform was purchased from Acros Organics. LC-MS grade methanol and LC-MS grade ammonium acetate were from Fluka. LC-MS grade water was purchased from Biosolve (Valkenswaard, Netherlands).

### Lipid Extraction Protocols

Lipid extracts were prepared using the MTBE protocol (Matyash et al., 2008). Briefly, 15 mg ground liver tissue was resuspended in 100 μl H$_2$O. The suspension was transferred into a 2 ml Eppendorf tube. 360 μl methanol and a mix of internal standards were added (400 pmol DLPC, 1000 pmol PE31:1, 1000 pmol PI31:1, 3300 pmol PS31:1, 2500 pmol C12SM, 500 pmol C17Cer and 100 pmol C8GC). Samples were vortexed and 1.2 ml of MTBE was added. Samples were placed for 10 min on a multitube vortexer at 4°C (Lab-tek International, Christchurch, New Zealand) followed by an incubation for 1 hr at room temperature (RT) on a shaker. Phase separation was induced by addition of 200 μl MS-grade water. After 10 min of incubation at RT samples were centrifuged at 1000 g for 10 min. The upper (organic) phase was transferred into a 13 mm glass tube with a Teflon-lined cap and the lower phase was reextracted with 400 μl artificial upper phase (MTBE / methanol / H$_2$O 10:3:1.5). In total 1500 μl of organic phase was recovered from each samples, split into three parts and dried in a CentriVap Vacuum Concentrator (Labconco, MO, USA). One part was treated by alkaline hydrolysis to enrich for sphingolipids and the other two aliquots were used for glycerophospholipid/phosphorus assay and sterol analysis, respectively.

Glycerophospholipids were deacylated according to the method by Clarke (Clarke and Dawson, 1981). Briefly, 1 ml freshly prepared monomethylamine reagent (methylamine/H$_2$O/n-butanol/methanol at 5:3:1:4 (vol/vol)) was added to the dried lipid extract and then incubated at 53°C for 1 hr in a water bath. Lipids were cooled to RT and then dried. For desalting, the dried lipid extract was resuspended in 300 μl water-saturated n-butanol and then extracted with 150 μl H$_2$O. The organic phase was collected, and the aqueous phase was reextracted twice with 300 μl water-saturated n-butanol. The organic phases were pooled and dried in a CentriVap Vacuum Concentrator.

### Determination of Total Phosphorus

The dried total lipid extract was resuspended in 250 μl chloroform/methanol (1:1) and 50 μl were placed into a 13 mm disposable pyrex tube. The solvent was completely evaporated and 0, 2, 5, 10, 20 μl of a 3 mM KH$_2$PO$_4$ standard solution were placed into separate pyrex tubes. To each tube 20 μl of water and 140 μl of 70% perchloric acid were added. Samples were heated at 180°C for 1 hr in a hood. Tubes were then removed from the block and kept at RT for 5 min. Then 800 μl of freshly prepared H$_2$O / 1.25% NH$_4$-Molybdate (100 mg / 8 ml H$_2$O) / 10% ascorbic acid (100 mg / 6 ml H$_2$O) in the ratio of 5:2:1 were added. Tubes were heated at 100°C for 5 min with a marble on each tube to prevent evaporation. Tubes were cooled at RT for 5 min. 100 μl of each sample was then transferred into a 96-well microplate and the absorbance at 820 nm was measured.

### Phospho- and Sphingolipid Analysis by Tandem Mass Spectrometry

Tandem mass spectrometry for the identification and quantification of phospho- and sphingolipid molecular species was performed using multiple reaction monitoring (MRM) with a TSQ Vantage Triple Stage Quadrupole Mass Spectrometer (Thermo Fisher Scientific) equipped with a robotic nanoflow ion source, Nanomate HD (Advion Biosciences, Ithaca, NY). Each individual ion dissociation pathway was optimized with regard to collision energy. Lipid concentrations were calculated relative to the relevant internal standards and then normalized to the total phosphate content of each total lipid extract.

## Sterol Analysis by Gas Liquid Chromatography Mass Spectrometry

Extracts were analyzed by GC–MS as described (Guan et al., 2010). Briefly, samples were injected into a VARIAN CP-3800 gas chromatograph equipped with a Factor Four Capillary Column VF-5 ms 15 m × 0.32 mm i.d. DF = 0.10 and analyzed by a Varian 320-MS triple quadrupole (Agilent Technologies) with electron energy set to – 70 eV at 250°C. Samples were applied with the column oven at 45°C, held for 4 min, then raised to 195°C (20°C / min). Sterols were eluted with a linear gradient from 195 to 230°C (4°C / min), followed by raising to 320°C (10°C / min). Finally, the column temperature was raised to 350°C (6°C / min) to elute sterol esters. Cholesterol and cholesterol esters were identified by their retention times (compared to standards) and fragmentation patterns, which were compared to the NIST library.

## Analysis of Total Fatty Acids

Normal chow (NC), coconut oil enriched high-fat diet (HFD-CO) and lard high-fat diet (HFD-L) were extracted with the MTBE lipid extraction protocol. Lipids were resuspended in 0.6 ml 14% boron trifluoride ($BF_3$) in methanol (Sigma-Aldrich) and vortexed. The tubes were incubated at 90°C for 4 min in a water bath and then placed on ice. The solution was transferred to an eppendorf tube and 100 µl of saturated NaCl solution was added. After vortexing 400 µl of hexane was added. The solution was vortexed, centrifuged (3000 g, 5 min) and the upper phase was transferred to a glass tube. The lower phase was reextracted twice with hexane (400 µl hexane and 200 µl hexane). The combined upper phases were dried with nitrogen. The dried lipids were resuspended in 500 µl hexane and further diluted 1:20 for GC-MS analysis. Samples were injected into a VARIAN CP-3800 gas chromatograph equipped with a Factor Four Capillary Column and analyzed by a Varian 320-MS triple quadrupole (Agilent Technologies). Samples were applied with the column oven at 45°C, held for 4 min, then raised to 130°C (20°C / min). Fatty acid methyl esters were eluted with a linear gradient from 130 to 205°C (3°C / min) followed by a final temperature rise to 350°C (40°C / min). Esterified fatty acids were identified by their retention times compared to the GLC-40 and GLC-50 FAME mix standards (Sigma-Aldrich) and by matching their mass spectra to the NIST library.

## Molecular Modeling

The docking of C12 and C16 in the ligand binding domain of PPARα, β/δ and γ was performed using three different software: Autodock 4 (Morris et al., 2009), Autodock Vina (Trott and Olson, 2010), and a developmental algorithm called "Attracting cavities" that will be implemented in EADock (Grosdidier et al., 2009, 2011). In brief, in the latter, an extended conformation of the ligand is minimized in the cavities of the protein, starting from different positions and orientations, in an approach similar to that of MCSS (Miranker and Karplus, 1991). Minimized poses are finally clustered and ranked according to the scoring function of EADock (Zoete et al., 2010). A detailed description of this algorithm will be the subject of a future communication.

All docking runs were performed using experimental X-ray structures of the binding domain of human PPARα (PDB [Rose et al., 2013] ID 1K7L [Xu et al., 2001]), PPARβ/δ (PDB ID 3SP9 [Jin et al., 2011]), and PPARγ (PDB ID 3V9Y [Furukawa et al., 2012]), after removing the ligand. The experimental binding assays on PPARα and PPARβ/δ were done using mouse proteins. However, since no experimental structure of a mouse PPAR is available, and in view of the high sequence conservation between the same isoforms of mouse and human PPARs in the ligand binding domain (92 to 96%), all docking runs were performed using experimental 3D structures of the latter. All residues mentioned to play a role in the predicted binding modes of C12 and C16 are conserved in the same isoforms of the mouse and human proteins.

Dockings were performed in a $25^3$ $\mathring{A}^3$ cubic box centered on the center of the ligand originally present in the PDB files. The so-defined search spaces cover entirely the binding pocket of PPAR, including the pocket entrance(Zoete et al., 2007). Autodock calculations were performed using 100 GA runs, each involving a maximum of 12'500'000 energy calculations. Vina calculations were performed using an exhaustiveness value of 100. Default values were used for all other parameters.

Since Arg280 of PPARγ, respectively Arg271 in PPARα, is flexible and adopts different conformation in the 1K7L and 3V9Y experimental structures, two additional docking runs were performed, in which the 1K7L conformation of this residue was adopted in the 3V9Y structure, and vice versa. The corresponding residue in PPARβ/δ, i.e., His244, is surrounded by other PPAR residues that prevent conformational changes.

### SUPPLEMENTAL REFERENCES

Clarke, N.G., and Dawson, R.M. (1981). Alkaline O leads to N-transacylation. A new method for the quantitative deacylation of phospholipids. Biochem. J. *195*, 301–306.

Furukawa, A., Arita, T., Fukuzaki, T., Satoh, S., Mori, M., Honda, T., Matsui, Y., Wakabayashi, K., Hayashi, S., Araki, K., and Ohsumi, J. (2012). Substituents at the naphthalene C3 position of (-)-Cercosporamide derivatives significantly affect the maximal efficacy as PPARγ partial agonists. Bioorg. Med. Chem. Lett. *22*, 1348–1351.

Grosdidier, A., Zoete, V., and Michielin, O. (2009). Blind docking of 260 protein-ligand complexes with EADock 2.0. J. Comput. Chem. *30*, 2021–2030.

Grosdidier, A., Zoete, V., and Michielin, O. (2011). Fast docking using the CHARMM force field with EADock DSS. J. Comput. Chem. Published online May 3, 2011. http://dx.doi.org/10.1002/jcc.21797.

Guan, X.L., Riezman, I., Wenk, M.R., and Riezman, H. (2010). Yeast lipid analysis and quantification by mass spectrometry. Methods Enzymol. *470*, 369–391.

Jin, L., Lin, S., Rong, H., Zheng, S., Jin, S., Wang, R., and Li, Y. (2011). Structural basis for iloprost as a dual peroxisome proliferator-activated receptor alpha/delta agonist. J. Biol. Chem. *286*, 31473–31479.

Matyash, V., Liebisch, G., Kurzchalia, T.V., Shevchenko, A., and Schwudke, D. (2008). Lipid extraction by methyl-tert-butyl ether for high-throughput lipidomics. J. Lipid Res. *49*, 1137–1146.

Miranker, A., and Karplus, M. (1991). Functionality maps of binding sites: a multiple copy simultaneous search method. Proteins *11*, 29–34.

Morris, G.M., Huey, R., Lindstrom, W., Sanner, M.F., Belew, R.K., Goodsell, D.S., and Olson, A.J. (2009). AutoDock4 and AutoDockTools4: Automated docking with selective receptor flexibility. J. Comput. Chem. *30*, 2785–2791.

Rose, P.W., Bi, C., Bluhm, W.F., Christie, C.H., Dimitropoulos, D., Dutta, S., Green, R.K., Goodsell, D.S., Prlic, A., Quesada, M., et al. (2013). The RCSB Protein Data Bank: new resources for research and education. Nucleic Acids Res. *41*(Database issue), D475–D482.

Trott, O., and Olson, A.J. (2010). AutoDock Vina: improving the speed and accuracy of docking with a new scoring function, efficient optimization, and multi-threading. J. Comput. Chem. *31*, 455–461.

Xu, H.E., Lambert, M.H., Montana, V.G., Plunket, K.D., Moore, L.B., Collins, J.L., Oplinger, J.A., Kliewer, S.A., Gampe, R.T., Jr., McKee, D.D., et al. (2001). Structural determinants of ligand binding selectivity between the peroxisome proliferator-activated receptors. Proc. Natl. Acad. Sci. USA *98*, 13919–13924.

Zoete, V., Grosdidier, A., Cuendet, M., and Michielin, O. (2010). Use of the FACTS solvation model for protein-ligand docking calculations. Application to EADock. J. Mol. Recognit. *23*, 457–461.

Zoete, V., Grosdidier, A., and Michielin, O. (2007). Peroxisome proliferator-activated receptor structures: ligand specificity, molecular switch and interactions with regulators. Biochim. Biophys. Acta *1771*, 915–925.
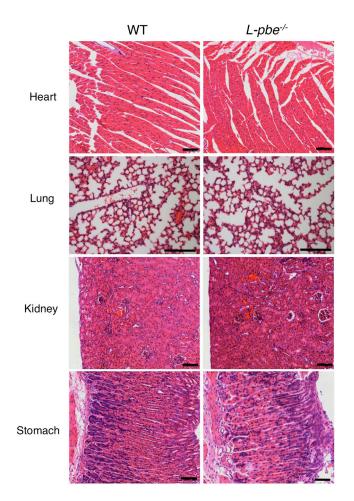
**Figure S1. Hematoxylin and Eosin-Stained Sections from Heart, Lung, Kidney, and Stomach, Related to Figure 1**
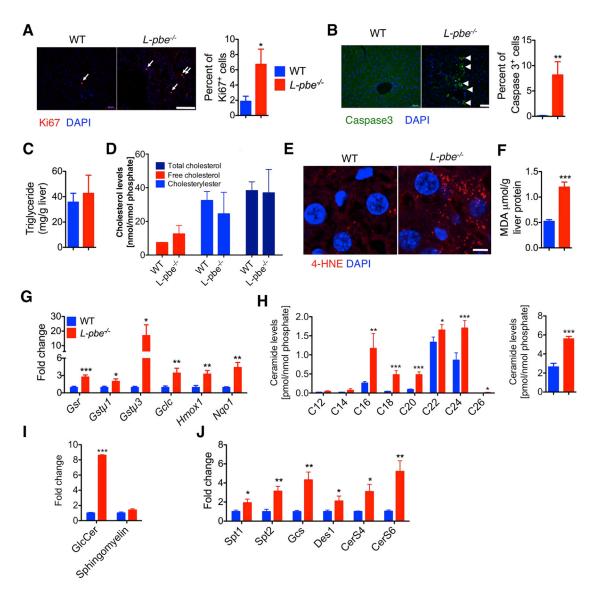Scale bar, 100 μm.

**Figure S2. Oxidative Stress and Ceramide Accumulation in the Liver of HFD-CO-Fed *L-pbe*^{−/−} Mice, Related to Figure 1**

(A) Hepatocyte proliferation (Ki67 labeling) and (B) apoptosis (caspase 3 stained cells) in livers of HFD-CO fed WT and *L-pbe*^{−/−} mice, Scale bar, 100 μm.

(C and D) (C) Triglyceride and (D) cholesterol levels in the livers from mice fed HFD-CO. Values are means ± SEM, n = 6.

(E) Immunohistochemical detection of 4-hydroxynonenal (4-HNE) protein adducts. Scale bar, 5 μm.

(F) Hepatic malondialdehyde (MDA) content.

(G) Hepatic expression of antioxidant phase II genes.

(H and I) Hepatic concentrations of (H) ceramides, (I) glycosylceramides and sphingomyelins.

(J) mRNA levels of sphingolipid biosynthesis genes.

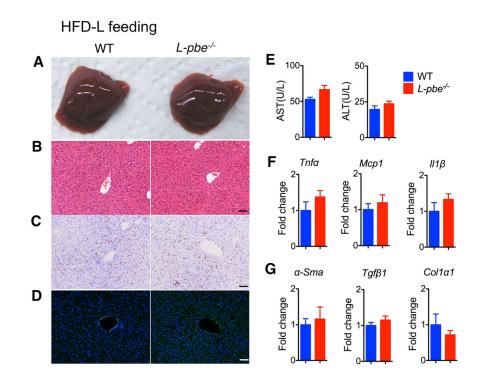Values are means ± SEM (n = 6-8, each group), *p < 0.05, **p < 0.01 and ***p < 0.001.

**Figure S3. Lard-Based HFD-L Does Not Induce Liver Damage in *L-pbe*⁻/⁻ Mice, Related to Figure 1**

(A) Livers from WT and *L-pbe*⁻/⁻ mice fed a HFD-L for 14 days.

(B) Hematoxylin and eosin staining.

(C) F4/80 immunostaining.

(D) α-smooth muscle actin immunostaining. Scale bars, 100 μm.

(E–F) (E) Blood levels of aspartate (AST) and alanine (ALT) aminotransferases, and hepatic expression levels of mRNAs for (F) proinflammatory cytokines, and (G) fibrosis markers.
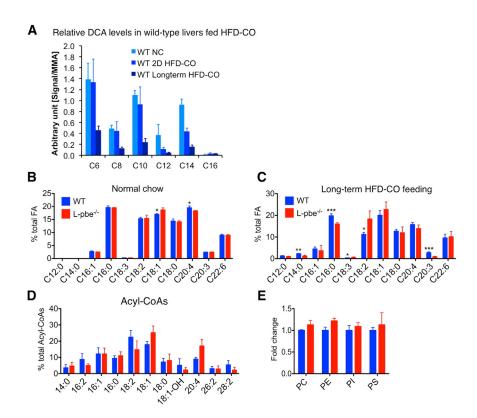
Values are means ± SEM, n = 6.

**Figure S4. Lipidomic Analysis of the Livers of WT and *L-pbe*<sup>−/−</sup> Mice Fed NC or HFD-CO, Related to Figure 2**

(A) Relative DCA levels in wild-type mice fed with normal chow or HFD-CO for short or long term.

(B and C) Fatty acids converted to their fatty acid methyl esters (FAMEs) after lipid extraction of livers from mice fed a normal chow (B) or a HFD-CO (C).

(D and E) Fatty acyl-CoAs (D) and total phospholipids (E) from livers of mice fed a long-term HFD-CO.

PC, phosphatidylcholine. PE, phosphatidylethanolamine. PI, phosphatidylinositol. PS, phosphatidylserine. Values are means ± SEM, n = 4.
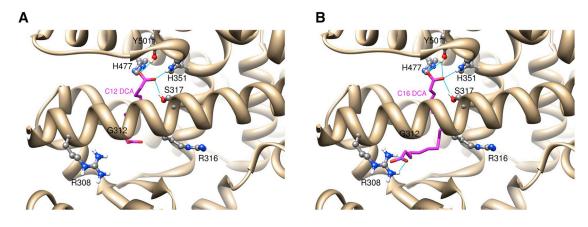
**Figure S5. Predicted Binding Mode of DCA for the Ligand Binding Domain of Human PPARγ, Related to Figure 4**

(A) Hypothetical binding mode of C12DCA to PPARγ showing that the reduced size of C12DCA makes simultaneous interaction with both R308 and the polar part of the binding site more difficult.

(B) C16DCA is shown in magenta and PPARγ as a tan ribbon, with important residues displayed in ball and stick. In this hypothesized binding mode, one carboxylate function of C16DCA binds the polar head of the ligand binding domain constituted by residues S317 (S280 in PPARα and T253 in PPARβ/δ), H351 (Y314 in PPARα and H287 in PPARβ/δ), H477 (H440 in PPARα and H413 in PPARβ/δ) and Y501 (Y464 in PPARα and Y437 in PPARβ/δ). The second carboxylate function is predicted to make ionic interactions with R308 (R271 in PPARα and H244 in PPARβ/δ). The aliphatic part of C16DCA extends in the hydrophobic binding pocket of PPAR, and exists by making non-polar interactions with G312 (C275 in PPARα). In PPARβ/δ, R308 of PPARγ is replaced by H244, which is already involved in an ionic interaction with E223, and is made inaccessible to an interaction with C16DCA due to the replacement of G312 in PPARγ by a bulky R248 in PPARβ/δ. The latter is also involved in ionic interactions with E223, and is not available to interact favorably with C16DCA. The lack of an available ionic interaction partner for the second carboxylate function of C16 and C12 DCA in PPARβ/δ could explain the inactivity of these compounds on the latter. All of the above-mentioned residues are conserved in the mouse proteins, as listed in Table S2.
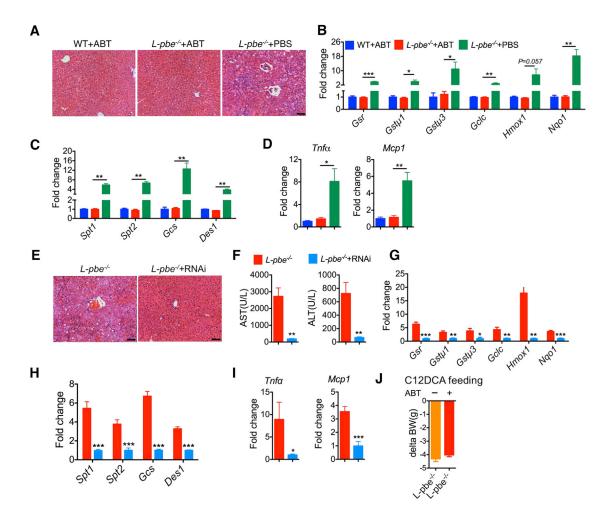
**Figure S6. Inhibiting DCA Production by Suppressing CYP4As Prevents Liver Failure in *L-pbe*$^{-/-}$ Mice, Related to Figure 6**

(A–D) Wild-type and *L-pbe*$^{-/-}$ mice were fed a HFD-CO diet and treated with ABT or PBS before collecting their livers for the following analysis: (A) Histology. (B) Phase II gene expression. (C) Sphingolipid biosynthesis gene expression. (D) Proinflammatory cytokine gene expression. PBS group: WT, n = 5; *L-pbe*$^{-/-}$, n = 11. ABT group: WT, n = 5; *L-pbe*$^{-/-}$, n = 13.

(E–I) siRNA-mediated knockdown of *Cyp4a*s prevents development of liver failure in HFD-CO fed *L-pbe*$^{-/-}$ mice. (E) Liver histology of mice treated with a control siRNA (*L-pbe*$^{-/-}$) or *Cyp4a*-specific siRNA (*L-pbe*$^{-/-}$+RNAi). (F) Plasma AST and ALT levels. (G) Antioxidant genes expression. (H) Sphingolipid synthesis genes expression. (I) Cytokine gene expression. Scale bar, 100 μm. *L-pbe*$^{-/-}$, n = 9; *L-pbe*$^{-/-}$ +RNAi, n = 12.

(J) Change in body weight of *L-pbe*$^{-/-}$ mice fed with a C12DCA-supplemented NC and simultaneously treated with saline or ABT.

Values are means ± SEM. *p < 0.05, **p < 0.01 and ***p < 0.001.